

Impact of velocity correlation and distribution on transport in fractured media: Field evidence and theoretical model

Peter K. Kang, Tanguy Le Borgne, Marco Dentz, Olivier Bour, Ruben Juanes

▶ **To cite this version:**

Peter K. Kang, Tanguy Le Borgne, Marco Dentz, Olivier Bour, Ruben Juanes. Impact of velocity correlation and distribution on transport in fractured media: Field evidence and theoretical model. Water Resources Research, 2015, 51 (2), pp.940-959. 10.1002/2014WR015799 . insu-01119364

HAL Id: insu-01119364
https://insu.hal.science/insu-01119364

Submitted on 23 Feb 2015

HAL is a multi-disciplinary open access archive for the deposit and dissemination of scientific research documents, whether they are published or not. The documents may come from teaching and research institutions in France or abroad, or from public or private research centers.

L'archive ouverte pluridisciplinaire **HAL**, est destinée au dépôt et à la diffusion de documents scientifiques de niveau recherche, publiés ou non, émanant des établissements d'enseignement et de recherche français ou étrangers, des laboratoires publics ou privés.

AGU PUBLICATIONS

Water Resources Research

RESEARCH ARTICLE

10.1002/2014WR015799

Key Points:
- Velocity distribution and correlation induce anomalous transport
- Field tracer experiments in fractured media show role of velocity correlation
- The proposed model incorporates both velocity distribution and correlation

Correspondence to:
T. Le Borgne,
tanguy.le-borgne@univ-rennes1.fr

Citation:
Kang, P. K., T. Le Borgne, M. Dentz, O. Bour, and R. Juanes (2015), Impact of velocity correlation and distribution on transport in fractured media: Field evidence and theoretical model, *Water Resour. Res.*, *51*, doi:10.1002/2014WR015799.

Received 2 MAY 2014
Accepted 6 DEC 2014
Accepted article online 15 DEC 2014

Impact of velocity correlation and distribution on transport in fractured media: Field evidence and theoretical model

Peter K. Kang[1], Tanguy Le Borgne[2], Marco Dentz[3], Olivier Bour[2], and Ruben Juanes[1]

[1]Department of Civil and Environmental Engineering, Massachusetts Institute of Technology, Cambridge, Massachusetts, USA, [2]Université de Rennes 1, CNRS, Geosciences Rennes, UMR 6118, Rennes, France, [3]Institute of Environmental Assessment and Water Research, Spanish National Research Council, Barcelona, Spain

Abstract Flow and transport through fractured geologic media often leads to anomalous (non-Fickian) transport behavior, the origin of which remains a matter of debate: whether it arises from variability in fracture permeability (velocity distribution), connectedness in the flow paths through fractures (velocity correlation), or interaction between fractures and matrix. Here we show that this uncertainty of distribution- versus correlation-controlled transport can be resolved by combining convergent and push-pull tracer tests because flow reversibility is strongly dependent on velocity correlation, whereas late-time scaling of breakthrough curves is mainly controlled by velocity distribution. We build on this insight, and propose a Lagrangian statistical model that takes the form of a continuous time random walk (CTRW) with correlated particle velocities. In this framework, velocity distribution and velocity correlation are quantified by a Markov process of particle transition times that is characterized by a distribution function and a transition probability. Our transport model accurately captures the anomalous behavior in the breakthrough curves for both push-pull and convergent flow geometries, with the same set of parameters. Thus, the proposed correlated CTRW modeling approach provides a simple yet powerful framework for characterizing the impact of velocity distribution and correlation on transport in fractured media.

1. Introduction

Understanding flow and transport through fractured geologic media is essential for improving forecasts, management, and risk assessment of many subsurface technologies, including geologic nuclear waste disposal [*Bodvarsson et al.*, 1999], geologic CO_2 storage [*Szulczewski et al.*, 2012], oil and gas production from fractured reservoirs [*Kazemi et al.*, 1976], enhanced geothermal systems [*Pruess*, 2006], shale-gas development [*Curtis*, 2002; *Cueto-Felgueroso and Juanes*, 2013], and groundwater contamination and remediation [*Gerke and van Genuchten*, 1993; *Huyakorn et al.*, 1994]. Moreover, if we conceptualize fractured geologic media as a network system, this knowledge can have implications to other physical processes, including disease spreading through river networks [*Rinaldo et al.*, 2012] and the air transportation system [*Nicolaides et al.*, 2012], urban traffic [*Kerner*, 1998], and nutrient transport through preferential paths in biofilms [*Wilking et al.*, 2013].

There are two main sources of uncertainty for transport through fractured media: uncertainty in the fracture geometrical properties, including fracture aperture, roughness, location, and connectivity describing fracture geometry [*Tsang et al.*, 1988; *Cacas et al.*, 1990; *Méheust and Schmittbuhl*, 2000; *de Dreuzy et al.*, 2001]; and uncertainty in the physical transport processes impacting the flow and transport such as advection, diffusion, dispersion, and adsorption [*Neretnieks*, 1983; *Haggerty and Gorelick*, 1995; *Becker and Shapiro*, 2003]. The fracture geometrical properties and the physical transport processes are interdependent, and may lead to anomalous transport. Anomalous transport, understood as the nonlinear scaling with time of the mean square displacement of transported particles, is a characteristic feature of transport through porous and fractured geologic media [*Berkowitz et al.*, 2006; *Bijeljic and Blunt*, 2006; *Berkowitz and Scher*, 1997].

Fracture geometrical properties impact macroscopic transport by controlling the velocity distribution at multiple scales. Fracture roughness leads to a broad velocity probability density function (PDF) at the fracture scale, and the variability in fracture aperture between fracture planes leads to a broad velocity PDF at the network scale [*Nordqvist et al.*, 1992; *Brown et al.*, 1998; *Méheust and Schmittbuhl*, 2000]. In the following,

© 2014. American Geophysical Union. All Rights Reserved.

we will refer to PDF as "probability distribution" or simply "distribution." In addition, fracture length impacts velocity correlation, since the velocity within each fracture is usually highly correlated. Therefore, the fracture geometrical properties impact both the transport velocity distribution and velocity correlation. In practice, however, the fracture geometrical information is very limited and only a few dominant properties, such as relative fracture aperture and dominant major fractures, are identifiable [*Dorn et al*., 2012].

Heterogeneous advection, matrix diffusion, hydrodynamic dispersion, and adsorption are four physical transport mechanisms that impact transport of nonreactive tracers through fractured media. Heterogeneous advection, which results from the separation of mass into different flow channels, can be partially reversible when the flow field is reversed. Matrix diffusion is a diffusive mass exchange between fractures and the surrounding rock matrix, which is not a time-reversible process. Hydrodynamic dispersion describes tracer spreading due to the combined effect of pore-fluid diffusion and local velocity heterogeneity within the fracture. Adsorption refers to the adhesion of dissolved tracers to solid surfaces. All these physical phenomena can be understood as either an advective or a diffusive process. Heterogeneous advection is an advective process, and matrix diffusion, hydrodynamic dispersion, and adsorption can be understood as diffusive processes. The competition between advective and diffusive processes is therefore manifested by the reversibility of flow, which in turn is controlled by velocity correlation. Advection is a time-reversible process: when flow is reversed, the spreading caused by heterogeneous advection collapses back. In contrast, diffusion is a time-irreversible process: particle spreading cannot be collapsed by reversing the flow. The advective versus diffusive-controlled breakthrough curve tailing has been tested by using tracers of different diffusivity and difference pumping rates [*Moench*, 1995; *Becker and Shapiro*, 2000; *Reimus and Callahan*, 2007]. These physical transport mechanisms also impact the Lagrangian velocity distribution. For example, heterogeneous advection induces a broad velocity distribution via the combination of slow paths and fast paths, matrix diffusion via the trapping of tracers in the rock matrix, and adsorption via the adhesion of particles onto the rock surface.

In summary, the complex interplay between fracture geometrical properties and physical transport processes determines the average particle transport behavior via velocity distribution and velocity correlation. Recent studies have shown that tracer transport through fractured and porous media is strongly modulated by the particle velocity distribution and velocity correlation [*Le Borgne et al*., 2008; *Kang et al*., 2011a; *de Anna et al*., 2013; *Kang et al*., 2014]. Here, we develop a stochastic model of transport that recognizes the impact of both velocity distribution and velocity correlation as an integral part of its ability to make predictions of transport at the field scale.

2. Field Experiments

A signature of anomalous transport in the field is the late-time tailing of breakthrough curves (BTCs), that is, time series of tracer concentration at the pumping well. Breakthrough curves are affected by both the underlying fracture geometrical properties and the physical transport processes such as advection, diffusion, dispersion, and adsorption. Thus, they are sensitive to both velocity distribution and velocity correlation.

We build on the seminal observation by *Tsang* [1995], who suggested that the combination of different tracer tests could be used to reduce the uncertainty in the characterization of fractured media. Here, we propose a framework to combine single-well (push-pull) and two-well (convergent) tests to give new constraints on distribution versus correlation-controlled non-Fickian transport.

2.1. Field Site and Tracer-Test Setup

We conducted a series of field tracer tests under forced hydraulic gradient in a saturated fractured granite formation at the Ploemeur observatory (H+ network) [*Le Borgne et al*., 2004; *Ruelleu et al*., 2010] (Figure 1). The site is located at the contact between the underlying fractured granite and the overlying mica schist. The matrix permeability of granite is extremely low and, therefore, groundwater flows mainly through the network of fractures.

For this study, we used two boreholes, B1 (83 m deep) and B2 (100 m deep), which are 6 m apart. Previous work [*Le Borgne et al*., 2007; *Dorn et al*., 2012, 2013] has identified four major conductive fractures intersecting B1, labeled B1-1 (24 m deep), B1-2 (50 m), B1-3 (63 m), and B1-4 (79 m), and four major conductive fractures intersecting B2, labeled B2-2 (56 m), B2-3 (59 m), B2-4 (79 m), and B2-5 (97 m). We designed and

© 2014. American Geophysical Union. All Rights Reserved.



Figure 1. (a) Outcrop of fractured granite at the Ploemeur field site. Inset: map showing the location of Ploemeur, France. (b) Photo from the installation of double packer system in B1 borehole.

conducted convergent and push-pull tests at two different fractures: B1-2 and B1-4. Regional flow may influence the reversibility of the flow [*Lessoff and Konikow*, 1997; *Altman et al*., 2002]. Direct measurements of ambient flow were obtained at the experimental site using the finite volume point dilution method using packers to isolate the fractures where the tracer tests were performed [*Brouyère et al*., 2008]. The ambient flow measured in B1-2 fracture was found to be below the detection limit (10^{-7} m^3/s), while that measured in B1-4 was about 10^{-6} m^3/s. Although these are local estimates, this suggests that ambient flow is too small ($\leq$ 0.06 L/min) to affect flow field generated by the injection/withdrawal rates (5–6 L/min). As a tracer, we used fluorescein, which is widely used for groundwater tracing and known to be nonreactive, insensitive to pH and salinity, and moderately resistant to adsorption and photochemical bleaching [*Smart and Laidlaw*, 1977].

2.1.1. Convergent Tracer Test

In the convergent test, we inject a known mass of tracer into an injection borehole (B1) and measure the tracer concentration at the pumping borehole (B2) (Figures 2a–2c). To place the tracer at the target fracture, we installed a double-packer at the injection borehole at two different depths, targeting the B1-2 and B1-4 fractures in separate experiments. To form a stationary, radial convergent flow configuration, a constant

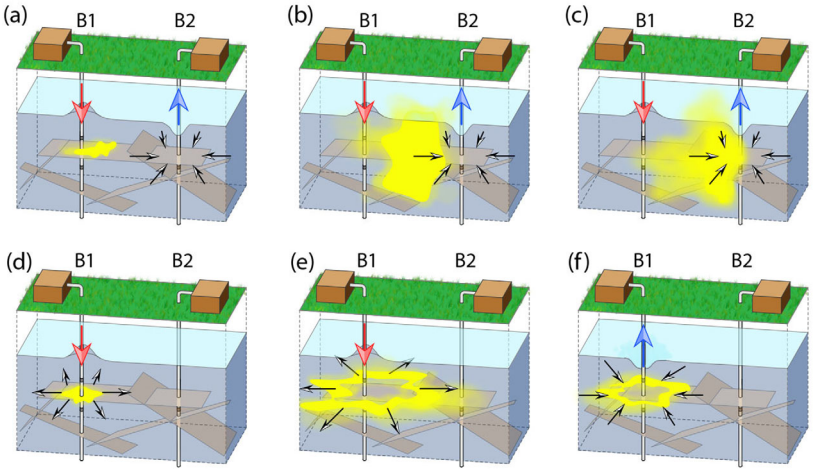


Figure 2. Schematic of the tracer tests conducted. (a,b,c) Convergent test with tracer placement at borehole B1 and pumping from borehole B2. Two different fracture planes at different depths (B1–2 and B1–4) are used for two separate tests. (d,e,f) Push-pull test from borehole B1. The same two fracture planes (B1–2 and B1–4) are used.

© 2014. American Geophysical Union. All Rights Reserved.

Table 1. Details of the Conditions and Parameters of the Four Tracer Experiments

	Experiments			
Experimental Parameters	B1–2 Convergent	B1–2 Push-Pull	B1–4 Convergent	B1–4 Push-Pull
Tracer injection fracture	B1–2	B1–2	B1–4	B1–4
Withdrawal borehole/fracture	B2	B1–2	B2	B1–4
Flow configuration	Convergent	Push-pull	Convergent	Push-pull
Tracer injection depth	50.5 m	50.5 m	78.7 m	78.7 m
Packer system at B1	Double packer	Double packer	Double packer	Double packer
Packer system at B2	Single packer	Single packer	Single packer	Single packer
Injection rate	1 L/min	6 L/min	1 L/min	5 L/min
Injection duration	15 min	30 min	15 min	80 min
Withdrawal rate	120 L/min	6 L/min	100 L/min	5 L/min
Injected mass	5 g	0.1 g	1.5 g	0.4 g
Peak arrival time	30 min	57 min	35 min	140 min
Peak concentration	590 ppb	353 ppb	312 ppb	690 ppb
Mass recovery	96 %	89 %	99 %	87 %
Late-time tailing slope	~ 1.7		~ 1.85	

pumping rate was established at borehole B2 throughout the experiment. Once a stationary pressure field is achieved, we inject the tracer at borehole B1 for a short duration compared to the total duration of the experiment, and at a small injection rate (<1% of the pumping rate at B2). When the injection of tracer is completed, we recirculate the fluid inside the double-packer system to prevent the possible remaining tracer from continuing to leak into the formation. We have monitored the well concentration during the experiment and confirmed the tracer concentration was small enough during the early stage of the experiment.

2.1.2. Push-Pull Tracer Test

In the push-pull test, we first inject a known mass of tracer into borehole B1, and continue to inject fresh water for a fixed duration of time ("push" phase). We then reverse the flow and pump water from the same borehole with the same flow rate ("pull" phase), and measure the arrival tracer concentration (Figures 2d-2f). Again, a double-packer system was installed to isolate the injection into the desired fracture plane.

2.2. Field Test Results

Additional details on the conditions and parameters of the field experiments are given in Table 1, and the measured BTCs are shown in Figure 3. As expected, the BTCs are broader for the convergent tests than for the push-pull tests, given that in the latter the spreading during the "push" phase is partially recovered

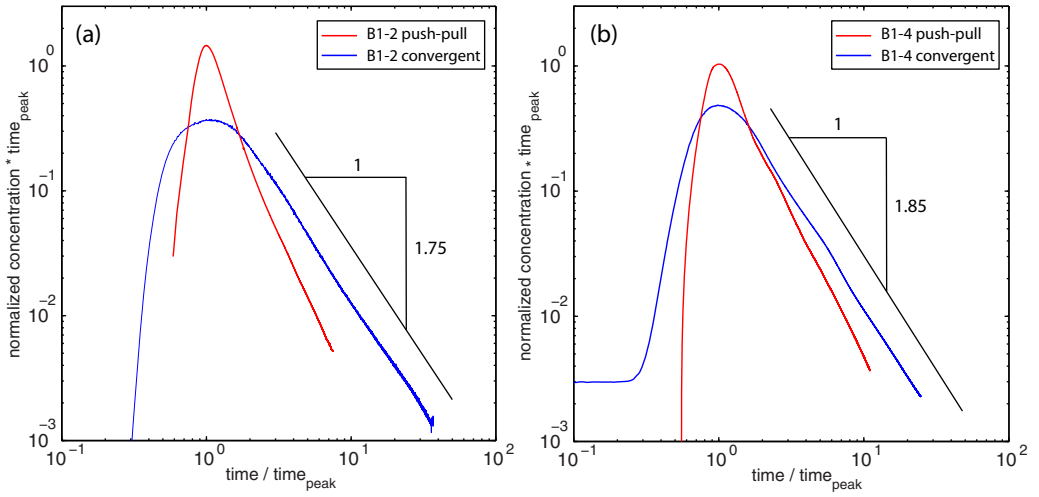


Figure 3. Measured breakthrough curves (BTC) for the tracer tests we conducted, in the form of a normalized time (peak arrival at dimensionless time of 1) and normalized concentration (such that the area under the BTC is identically equal to 1). The tracer concentration is measured every 20 s. (a) BTCs for fracture plane B1–2. (b) BTCs for fracture plane B1–4.

© 2014. American Geophysical Union. All Rights Reserved.

during the "pull" phase. Indeed, the degree to which the initial tracer spreading is reversed is an indication of the strength of velocity correlation.

Analyzing the two convergent tests, we note that the power-law late-time scalings are different, exhibiting a slope of ~1.75 for B1-2 and ~1.85 for B1-4. This difference reflects different velocity distributions, and can be interpreted as different levels of heterogeneity. The gentler slopes in the BTCs indicate a broader range (higher probability) toward small velocities.

Motivated by these field observations, we review existing theoretical transport models, and develop a new model that takes into account both velocity distribution and velocity correlation.

3. Existing Models of Transport

Various approaches have been proposed to model flow and transport through fractured media, ranging from equivalent porous medium approaches that represent the fractured medium as a single continuum [*Neuman et al*., 1987; *Tsang et al*., 1996], to discrete fracture networks that explicitly represent fractures as entities embedded in the surrounding matrix [*Kiraly*, 1979; *Cacas et al*., 1990; *Moreno and Neretnieks*, 1993; *Juanes et al*., 2002; *Molinero et al*., 2002; *Karimi-Fard et al*., 2004; *Martinez-Landa and Carrera*, 2005; *Molinero and Samper*, 2006; *Martinez-Landa et al*., 2012; *de Dreuzy et al*., 2012a; *Schmid et al*., 2013]. Dual-porosity models are, in some sense, in between these two extremes, and conceptualize the fractured-porous medium as two overlapping continua, which interact via an exchange term [*Bibby*, 1981; *Feenstra et al*., 1985; *Maloszewski and Zuber*, 1985; *Gerke and van Genuchten*, 1993].

Stochastic models that account for the observed non-Fickian global transport behavior in fractured media include continuous-time random walks (CTRW) [*Berkowitz and Scher*, 1997; *Geiger et al*., 2010; *Kang et al*., 2011b,a], fractional advection-dispersion equations (fADE) [*Benson et al*., 2000], multirate mass transfer (MRMT) [*Haggerty and Gorelick*, 1995; *Carrera et al*., 1998; *Le Borgne and Gouze*, 2008], stochastic convective stream tube (SCST) models [*Becker and Shapiro*, 2003], and Boltzmann equation approaches [*Benke and Painter*, 2003]. All of these models are valid under their own assumptions and have played an important role in advancing the understanding of transport through fractured media. Among these models, the MRMT and SCST approaches have been applied to model non-Fickian tracer transport in both push-pull and convergent tests at the same site [*Haggerty et al*., 2001; *McKenna et al*., 2001; *Becker and Shapiro*, 2003].

Below, we briefly revisit the basic formulations of the classical advection-dispersion, stochastic-convective streamtube, and multirate mass transfer models for radial flow geometries, and discuss their ability to capture BTCs for convergent and push-pull tests.

3.1. Advection-Dispersion Equation (ADE) Model

The classical advection-dispersion equation (ADE) in radial coordinates is given by

$$\frac{\partial c(r,t)}{\partial t}+\frac{k_v}{r}\frac{\partial c(r,t)}{\partial r}-\frac{\alpha k_v}{r}\frac{\partial^2 c(r,t)}{\partial r^2}=0, \tag{1}$$

where α is dispersivity and $k_v=Q/(2\pi b_{\text{eff}})$ with Q the volumetric flow rate and b_{eff} the mass balance aperture. The mass balance aperture, b_{eff}, can be defined as $Q\langle\tau_a\rangle/\left(\pi\left([r(0)+r_c]^2-r(0)^2\right)\right)$ for a convergent tracer test, where $\langle\tau_a\rangle$ is the mean solute arrival time, $r(0)$ is the pumping point, and r_c the distance between the tracer injection point and the withdrawal point [*Tsang*, 1992]. The mass balance aperture, b_{eff}, represents an average aperture along the flow paths for tracer transport. Since we will use a Lagrangian modeling approach in the following, we formulate the advection-dispersion model in terms of radial particle trajectories. This can be done by rewriting (1) in terms of a conserved variable in radial coordinates,

$$p(r,t)=2\pi b_{\text{eff}} r c(r,t), \tag{2}$$

which is the particle density per unit radial length. Inserting the latter into (1) we obtain

$$\frac{\partial p(r,t)}{\partial t}+\frac{\partial}{\partial r}\frac{k_v}{r}p(r,t)-\frac{\partial^2}{\partial r^2}\frac{\alpha k_v}{r}p(r,t)=0. \tag{3}$$

The equivalent Langevin equation is given by

© 2014. American Geophysical Union. All Rights Reserved.

$$\frac{dr(t)}{dt} = \frac{k_v}{r(t)} + \sqrt{\frac{2\alpha k_v}{r(t)}}\xi_r(t), \tag{4}$$

where $\xi_r(t)$ is a Gaussian white noise of zero mean and unit variance. Here and in the following, we employ the Ito interpretation of the Langevin equation (4) [*Risken*, 1989]. The particle density is given in terms of the radial trajectories as $p(r,t)=\langle\delta[r-r(t)]\rangle$, and by virtue of (2), we obtain for the concentration distribution

$$c(r,t) = \frac{1}{2\pi b_{\text{eff}} r}\langle\delta[r-r(t)]\rangle. \tag{5}$$

The angular brackets $\langle\cdot\rangle$ denote the average over all solute particles.

The solute breakthrough curve at a distance r_c from the injection point $r(0)$ is given in terms of the probability density function of the particles' first arrival times at the radius $r=r(0)+r_c$,

$$\tau_a = \inf\{t|\,|r(t)-r(0)| \geq r_c\}, \tag{6}$$

which is defined by

$$f(\tau) = \langle\delta(\tau-\tau_a)\rangle. \tag{7}$$

The mean solute arrival time at a radius r_c is given by

$$\langle\tau_a\rangle = \frac{[r(0)+r_c]^2 - r(0)^2}{2k_v}, \tag{8}$$

which is also the peak arrival time.

3.2. Stochastic Convective Stream Tube (SCST) Model

Stochastic convective streamtube models assume that transport occurs along independent streamtubes. Transport within streamtubes is one-dimensional, and there is no mass exchange between individual streamtubes [*Dagan and Bressler*, 1979; *Cirpka and Kitanidis*, 2000; *Ginn*, 2001; *Becker and Shapiro*, 2003]. Thus, these models are sometimes called minimum mixing models. For uniform mean flow, transport in a single radial streamtube of type ω is given by [*Ginn*, 2001; *Becker and Shapiro*, 2003]

$$\frac{\partial c_\omega(x,t)}{\partial t} + \frac{k_\omega}{r}\frac{\partial c_\omega(r,t)}{\partial r} - \frac{\alpha k_\omega}{r}\frac{\partial^2 c_\omega(r,t)}{\partial r^2} = 0, \tag{9}$$

where k_ω is given by $k_\omega = Q_\omega/(2\pi b_\omega \phi_\omega)$ with Q_ω the flow rate, b_ω the typical aperture and ϕ_ω the porosity of the streamtube, and α is the dispersivity. The total solute concentration $c(r, t)$ is given by the average of $c_\omega(r,t)$ over all streamtubes

$$c(r,t) = \int d\omega \mathcal{P}(\omega) c_\omega(r,t), \tag{10}$$

where $\mathcal{P}(\omega)$ denotes the PDF of streamtubes. Macroscopic solute dispersion here is caused predominantly by velocity contrasts between streamtubes. Transport is fully reversible for $\alpha = 0$. The only irreversible transport mechanism in this framework is dispersion along the streamtubes.

The Lagrangian formulation of transport in a single streamtube ω is identical to (4) because transport along a streamtube is given by the radial advection-dispersion equation (9). In many realistic flow and transport scenarios, radial dispersion can be disregarded because its effect on solute spreading is negligible compared with advective heterogeneity. For $\alpha = 0$, the Langevin equation (4) for a single streamtube ω reduces to

$$\frac{dr_\omega(t)}{dt} = \frac{k_\omega}{r_\omega(t)}. \tag{11}$$

Consequently, in the case of an instantaneous solute injection, and using (5), we obtain the following expression for the total solute concentration (10),

© 2014. American Geophysical Union. All Rights Reserved.

$$c(r,t)=\frac{1}{2\pi br}\int d\omega \mathcal{P}(\omega)\phi_\omega^{-1}\delta[r-r_\omega(t)]. \tag{12}$$

The solute arrival time τ_ω at a distance r_c in a single streamtube is given by

$$\tau_\omega=\frac{[r_c+r(0)]^2-r(0)^2}{2k_\omega}. \tag{13}$$

The total solute breakthrough is given by averaging the deterministic arrival times τ_ω over the ensemble of streamtubes, which is characterized by the distribution $\mathcal{P}_{k_\omega}(k)$ of k_ω,

$$f(\tau)=\int dk \mathcal{P}_{k_\omega}(k)\delta[\tau-\tau_\omega(k)]. \tag{14}$$

For a push-pull tracer test, we immediately see that the breakthrough curve is given by $f(\tau)=\delta(t-2t_p)$, where t_p is the push time. The solute arrival time at the injection point is simply twice the push time because of the full reversibility of transport, as described by (11).

3.3. Multirate Mass Transfer (MRMT) Model

The MRMT model considers solute transport under mass transfer between a single mobile zone and a series of immobile zones. Fast solute transport in the mobile zone and solute retardation in the immobile zones can lead to non-Fickian spatial distributions and breakthrough curves, and in general to an increase of solute dispersion. Solute mass conservation in the mobile domain is expressed in radial coordinates by

$$\phi_m\frac{\partial c_m(r,t)}{\partial t}+\frac{\phi_m k_v}{r}\frac{\partial c_m(r,t)}{\partial r}-\frac{\alpha\phi_m k_v}{r}\frac{\partial^2 c_m(r,t)}{\partial r^2}=-\phi_{im}\frac{\partial c_{im}(r,t)}{\partial t} \tag{15}$$

where ϕ_m and ϕ_{im} are the (average) porosities of the mobile and immobile continua, respectively, $k_v=Q/(2\pi b\phi_m)$ with Q the flow rate and b the width of the injection interval, and α is the dispersivity. Mass transfer between the mobile and immobile regions is linear and thus, assuming zero initial conditions in the immobile regions, the mobile $c_m(r,t)$ and immobile $c_{im}(r,t)$ solute concentrations are related by [*Dentz and Berkowitz*, 2003]

$$c_{im}(r,t)=\int_0^t dt'\varphi(t-t')c_m(r,t'), \tag{16}$$

where $\varphi(t)$ is the memory function that encodes the specific mass transfer mechanism [*Haggerty and Gorelick*, 1995; *Harvey and Gorelick*, 1995; *Carrera et al*., 1998; *Dentz and Berkowitz*, 2003; *Dentz et al*., 2011a]. For linear first-order mass exchange, $\varphi(t)$ determines the distribution of transfer rates between mobile and immobile regions [*Haggerty and Gorelick*, 1995]. For diffusive mass transfer, it encodes the geometries and the characteristic diffusion scales of the immobile regions [*Dentz et al*., 2011a]. Combining (15) and (16), we write the temporally nonlocal single-equation MRMT model

$$\begin{aligned}\phi_m\frac{\partial c_m(r,t)}{\partial t}+\phi_{im}\frac{\partial}{\partial t}\int_0^t dt'\varphi(t-t')c_m(r,t')\\ +\frac{\phi_m k_v}{r}\frac{\partial c_m(r,t)}{\partial r}-\frac{\alpha\phi_m k_v}{r}\frac{\partial^2 c_m(r,t)}{\partial r^2}=0.\end{aligned} \tag{17}$$

It has been shown that the MRMT model is equivalent to CTRW models characterized by uncoupled transition length and time distributions, and to time fractional advection-dispersion models [*Dentz and Berkowitz*, 2003; *Schumer et al*., 2003; *Benson and Meerschaert*, 2009]. The MRMT model was employed by *Haggerty et al*. [2001] to intepret breakthrough curves for radial push-pull tracer tests in fractured dolomite. *Le Borgne and Gouze* [2008] used a CTRW implementation of MRMT to simulate breakthrough curves for radial push-pull tracer tests. The MRMT models and its equivalent CTRW and fADE formulations describe solute dispersion as an irreversible process. In these modeling frameworks, retardation events that essentially cause macroscopic solute dispersion are independent. Thus, transport is irreversible upon flow reversal.

As in the previous section, we formulate the radial MRMT model (17) in a Lagrangian framework. Following the approach employed in *Le Borgne and Gouze* [2008], we implement MRMT in terms of the continuous time random walk

© 2014. American Geophysical Union. All Rights Reserved.

$$r_{n+1}=r_n+\frac{k_v}{r_n}\Delta s+\sqrt{\frac{2\alpha k_v\Delta s}{r_n}}\xi_n, \tag{18a}$$

$$t_{n+1}=t_n+\Delta s+\eta_n\Delta s, \tag{18b}$$

where the ξ_n are identical independently distributed Gaussian random variables with zero mean and unit variance, and Δs is an operational time increment. The dimensionless random time increments η_n are identical independently distributed random variables with the distribution density $\psi(\eta)$. For $\eta_n \equiv 0$, the system (18) is identical to the discretized version of (4) in the Ito interpretation.

The continuous time random walk (18) is equivalent to (17) in the limit of small Δs with the identification [*Dentz and Berkowitz*, 2003]

$$\varphi(t)=\frac{\phi_m}{\phi_{im}}\mathcal{L}^{-1}\left\{\frac{1-\psi^*(\lambda\Delta s)(1+\lambda\Delta s)}{\lambda\Delta s\psi^*(\lambda\Delta s)}\right\}, \tag{19}$$

where $\mathcal{L}^{-1}\{\cdot\}$ denotes the inverse Laplace transform, $\psi^*(\lambda)$ is the Laplace transform of $\psi(t)$, and λ the Laplace variable. Here and in the following, Laplace-transformed quantities are marked by an asterisk.

The distribution of solute arrival times for both convergent and push-pull tracer tests is obtained from the individual particle arrival times $\tau_a=\inf(t_n|\,|r_n-r_0|>r_c)$ as

$$f(\tau)=\overline{\delta(\tau-\tau_a)}, \tag{20}$$

where the overbar $\overline{(\cdot)}$ denotes the average over the ensemble of all particles characterized by the stochastic series of dimensionless retention times $\{\eta_n\}$. Notice that the arrival time distribution in the push-pull case does not reduce to a delta-density, as in the SCST model. Solute transport is irreversible in the MRMT approach that we presented.

3.4. Comparison of ADE, SCST, and MRMT Models

The traditional ADE formulation presented in subsection 3.1 does not have the ability to capture anomalous transport, manifested as a power-law tailing in BTCs. To overcome this limitation, SCST and MRMT models have been applied to explain BTCs for convergent and push-pull tests. To show the fundamental difference between the two models, we run both convergent and push-pull simulations with the two models. For the MRMT model, we employ the Pareto waiting time distribution

$$\psi(\eta)=\frac{\beta}{\eta_0}\left(\frac{\eta}{\eta_0}\right)^{-1-\beta},\ \eta>\eta_0, \tag{21}$$

with $0<\beta<2$. For the distribution of the k_ω in the SCST approach we employ the distribution

$$\mathcal{P}_{k_\omega}(k)=\frac{\beta}{k_0}\left(\frac{k}{k_0}\right)^{\beta-1},\ k<k_0. \tag{22}$$

The distributions (21) and (22) for the MRMT and SCST models, respectively, give identical slopes for the long time behavior of the BTCs in the convergent tracer tests. In Figure 4, we show the modeling results for MRMT and SCST models. We can see the clear distinction between the two models. Since MRMT does not have a mechanism to capture the reversibility of advective spreading, the BTCs of convergent and push-pull tests are almost identical. In contrast, the stream tube model assumes perfect correlation in velocity, and we observe perfect reversibility in the BTC for the push-pull tracer test in the absence of local dispersion within streamtubes. In reality, there always exists both irreversible diffusive and reversible advective processes, and our objective is to develop a stochastic model that recognizes the competition between the two processes.

The limitations of MRMT and SCST (as well as ADE and classical CTRW) in reproducing the time-reversibility behavior of both types of tracer tests could be relieved if the models were applied in multidimensions, with spatially variable permeability fields. This, however, would rapidly increase model complexity, the number of model parameters, and would require more field data to reliably constrain those parameters. The objective of our work is to propose a parsimonious theoretical model that accounts for reversible and irreversible processes in 1-D radial coordinates.

© 2014. American Geophysical Union. All Rights Reserved.

4. Continuous Time Random Walks (CTRW) With Correlated Velocities

As discussed in subsection 3.4, the SCST and MRMT frameworks represent transport models that exhibit full reversibility and complete irreversibility, respectively. The breakthrough curves obtained from convergent and push-pull tracer tests at the Ploemeur fractured aquifer, however, exhibit neither full reversibility nor complete irreversibility (Figure 3). Here we develop a stochastic model based on a correlated CTRW approach [*Le Borgne et al.*, 2008; *Kang et al.*, 2011a; *de Anna et al.*, 2013; *Kang et al.*, 2014], with the following two design criteria: Lagrangian velocity correlation that captures flow reversibility, and particle velocity distribution that captures velocity heterogeneity.

4.1. Model Formulation

The starting point for the model is the Langevin equation (4) in differential form

$$dr(t)=\frac{k_v dt}{r(t)}+\sqrt{2\alpha\frac{k_v dt}{r(t)}}\xi_r(t). \tag{23}$$

By defining the differential space increment $d\vartheta=k_v dt/r(t)$ [*Dentz et al.*, 2009; *Dentz and Bolster*, 2010], equation (23) transforms into

$$dr(\vartheta)=d\vartheta+\sqrt{2\alpha d\vartheta}\xi_r(\vartheta), \tag{24a}$$

$$dt(\vartheta)=\frac{r(\vartheta)}{k_v}d\vartheta. \tag{24b}$$

Discretizing this system in ϑ and setting $\Delta\vartheta=\ell$ gives the following system of equations for the particle trajectories in space and time coordinates, or in other words, a CTRW,

$$r_{n+1}=r_n+\ell+\sqrt{2\alpha\ell}\xi_n, \tag{25a}$$

$$t_{n+1}=t_n+\frac{\ell r_n}{k_v}. \tag{25b}$$

Notice that this CTRW is characterized by a radially dependent time increment. It is by definition equivalent to (3) in the limit of small $\ell \ll L$, with L a macroscopic observation scale.

We generalize this CTRW heuristically in order to account for variability in radial particle velocities that may be induced by spatial variability in hydraulic conductivity and retardation properties of the medium. Notice that the transport velocity depends on both hydraulic conductivity and porosity. *Le Borgne et al.* [2008] and *Kang et al.* [2011a] demonstrated that the impact of flow heterogeneity on large-scale solute transport can be quantified in terms of CTRWs whose time increments form a Markov chain based on the observation that the series of Lagrangian particle velocities form a Markov process.

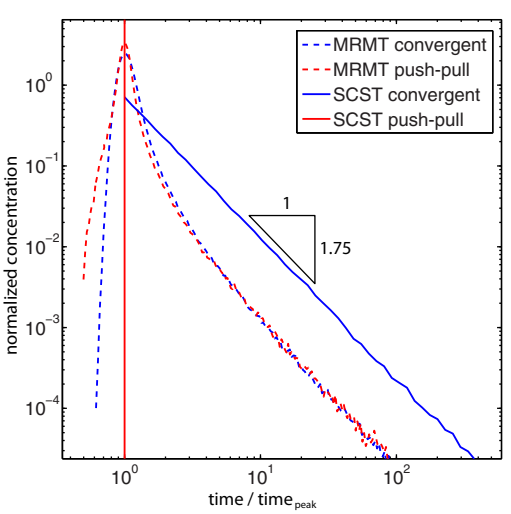


Figure 4. Comparison of the breakthrough curves (BTC) for the MRMT and SCST models characterized by the distributions (21) and (22) with $\beta=1.75, \eta_0=0.005$ and $k_0=200$, respectively. The BTCs for the convergent and push-pull scenarios are almost identical in the MRMT approach because solute spreading is irreversible. In contrast, the BTC for the convergent and push-pull scenarios in the SCST model are drastically different: in the absence of local dispersion, the BTC in the push-pull scenario is a delta distribution due to the perfect velocity correlation within each streamtube, i.e., full reversibility.

We define here a radial-correlated CTRW that allows to vary the velocity correlation (persistence of particle velocities) and velocity distribution (PDF of particle velocities), to represent and quantify both correlation and distribution-

© 2014. American Geophysical Union. All Rights Reserved.

induced anomalous transport features, and to discriminate between them [*Dentz and Bolster*, 2010]. Thus, we generalize the stochastic process (25b) of particle times according to

$$t_{n+1}=t_n+\frac{\ell r_n}{k_v}\eta_n, \tag{25c}$$

where the dimensionless time increments $\{\eta_n\}$ form a Markov chain characterized by the marginal distribution density $\psi_0(\eta)$ of initial increments η_0 and the one-step transition probability density $\psi_1(\eta|\eta')$. The Chapman-Kolmogorov equation for the *n*-step transition time density $\psi_n(\eta|\eta')$ reads

$$\psi_n(\eta|\eta')=\int_0^\infty d\eta''\psi_{n-m}(\eta|\eta'')\psi_m(\eta''|\eta'). \tag{26}$$

The density $\psi_n(\eta)$ of random increments η_n after *n* steps is given by

$$\psi_n(\eta)=\int_0^\infty d\eta'\psi_n(\eta|\eta')\psi_0(\eta'). \tag{27}$$

We set here $\psi_0(\eta)=\psi(\eta)$ equal to the steady state density, which is an eigenfunction of the transition density $\psi_1(\eta|\eta')$ and therefore $\psi_n(\eta)=\psi(\eta)$. This is equivalent to assuming that particles sample velocities from the steady state Lagrangian velocity distribution from the beginning. Equations (25a) and (25c) constitute the equations of motion of solute particles in the proposed radial correlated CTRW approach, where $\psi(\eta)$ determines the velocity distribution and $\psi_1(\eta|\eta')$ determines the velocity correlation.

4.2. Limiting Cases

In the following, we briefly determine the limits of the system (25a) and (25c) for fully correlated and fully uncorrelated dimensionless time increments $\{\eta_n\}$.

4.2.1. Fully Correlated Case

In the limit of fully correlated $\{\eta_n\}$, i.e., $\psi_1(\eta|\eta')=\delta(\eta-\eta')$, where δ denotes the Kronecker delta, equations (25a) and (25c) reduce to

$$r_{n+1}=r_n+\ell+\sqrt{2\alpha\ell}\xi_n, \tag{28a}$$

$$t_{n+1}=t_n+\frac{\ell r_n}{k_\omega}, \tag{28b}$$

where we defined the constant $k_\omega=k_v/\eta_\omega$ with η_ω the perfectly persistent increment, which is distributed according to $\psi(\eta)$. Each η_ω, or k_ω, represents a streamtube in the sense of the SCST model. In fact, just as (25a) and (25b) are equivalent to (3), so is system (28), which constitutes the equivalence of (28) and (9). Therefore, the fully correlated case of the proposed model is equivalent to the SCST model.

4.2.2. Fully Uncorrelated Case

In the limit of fully uncorrelated $\{\eta_n\}$, i.e., $\psi_1(\eta|\eta')=\psi(\eta)$, the system (25a) and (25b) is equivalent to the following nonlocal radial advection dispersion equation

$$\frac{\partial c(r,t)}{\partial t}+\int_0^t dt'\left[\frac{\phi k_v}{r}\frac{\partial}{\partial r}M(r,t-t')c(r,t')-\frac{\alpha\phi k_v}{r}\frac{\partial^2}{\partial r^2}M(r,t-t')c(r,t')\right]=0, \tag{29}$$

with the radially dependent memory function

$$M(r,t)=\mathcal{L}^{-1}\left\{\frac{\lambda\eta_k(r)\psi^*[\lambda\eta_k(r)]}{1-\psi^*[\lambda\eta_k(r)]}\right\}. \tag{30}$$

We defined $\eta_k(r)=\ell r/k_v$ for compactness. The memory function depends explicitly on the radial position through the radially dependent time scale $\eta_k(r)$. Notice that this radial CTRW model is in general different from the radial MRMT model (17).

4.3. Model Implementation

The proposed CTRW with correlated transition times (25a) and (25c) is solved using random walk particle tracking. The model has three key transport characteristics: the probability distribution of the dimensionless

© 2014. American Geophysical Union. All Rights Reserved.

time increments, $\psi(\eta)$, the one step transition probability that quantifies the velocity correlation, $\psi_1(\eta|\eta')$, and the local dispersivity, α. Here we present how to characterize $\psi(\eta)$ and $\psi_1(\eta|\eta')$, and explain in detail the random walk particle tracking algorithm used to solve for the BTCs in the convergent and push-pull scenarios.

4.3.1. Transition Probability and Correlation

To independently control velocity distribution and velocity correlation, we describe the Markov process $\{\eta_n\}$ with the steady state distribution, $\psi(\eta)$. The continuous nondimensional transition times η are discretized into N classes, $\eta \in \cup_{j=1}^{N}(\eta_j, \eta_{j+1}]$, such that the transition probabilities between the classes are represented by the $N \times N$ transition matrix $\mathbf{T}$, with components

$$T_{ij} = \int_{\eta_i}^{\eta_{i+1}} d\eta \int_{\eta_j}^{\eta_{j+1}} d\eta' \psi_1(\eta|\eta')\psi(\eta') \Big/ \int_{\eta_j}^{\eta_{j+1}} d\eta' \psi(\eta'). \tag{31}$$

The transition matrix satisfies $\mathbf{T}^{n+m} = \mathbf{T}^n\mathbf{T}^m$. Here, we choose equiprobable binning such that

$$\int_{\eta_i}^{\eta_{i+1}} d\eta \psi(\eta) = \frac{1}{N}. \tag{32}$$

With this condition, $\mathbf{T}$ is a doubly stochastic matrix, which therefore satisfies

$$\sum_{i=1}^{N} T_{ij} = \sum_{j=1}^{N} T_{ij} = 1. \tag{33}$$

For a large number of transitions, the transition matrix converges toward the uniform matrix,

$$\left[\lim_{n\to\infty} \mathbf{T}^n\right]_{ij} = \frac{1}{N}, \tag{34}$$

whose eigenvalues are 1 and 0. Thus, correlation can be measured by the convergence of $\mathbf{T}$ toward the uniform matrix. The correlation length is determined by the decay rate of the second largest eigenvalue χ_2 (the largest eigenvalue of a stochastic matrix is always 1). The correlation function is defined by $C(n) = \chi_2^n$, which can be written as

$$C(n) = \exp\left(-\frac{n}{n_c}\right), n_c = -\frac{1}{\ln(|\chi_2|)}, \tag{35}$$

where n_c is the correlation step number. Thus, we define the dimensionless correlation length λ as

$$\lambda = \frac{n_c \ell}{r_c} \tag{36}$$

with ℓ the spatial discretization of the correlated CTRW model. Note that the discretization length ℓ should be smaller than the velocity correlation length, λr_c.

Here we consider a simple transition matrix model, in which all diagonal entries are fixed to a constant a, and the remaining entries are equal to $(1-a)/(N-1)$,

$$T_{ij} = a\delta_{ij} + \frac{1-a}{N-1}(1-\delta_{ij}). \tag{37}$$

This transition matrix imposes the same correlation function for all starting velocities, and the diagonal value of $a \leq 1$ determines the correlation strength. A value of $a = 1$ implies perfect correlation, which renders the N-dimensional unity matrix, $T_{ij} = \delta_{ij}$. For $a = 1/N$, all transitions are equally probable, and the transition matrix is equal to the uniform matrix with $T_{ij} = 1/N$; see Figure 5b. The transition matrix (37) has the eigenvalues $\chi_1 = 1$ and

$$\chi_2 = \frac{Na-1}{N-1}, \tag{38}$$

such that we obtain for the dimensionless correlation length (36)

© 2014. American Geophysical Union. All Rights Reserved.

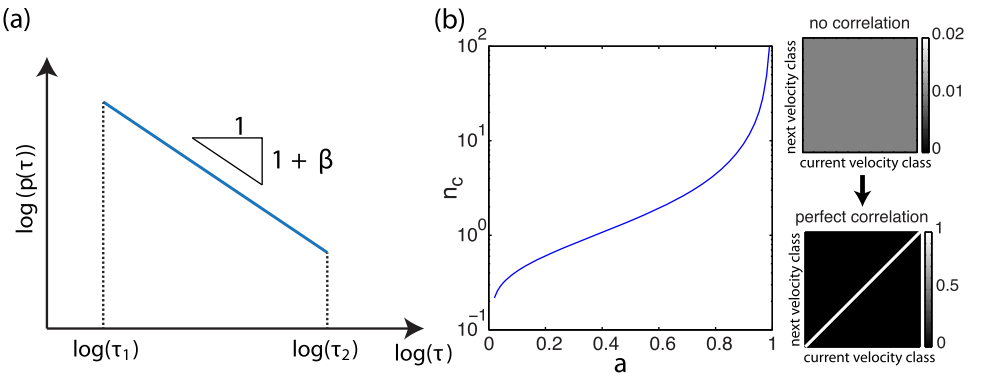


Figure 5. Key transport characteristics of our proposed CTRW model. (a) $\psi(\eta)$ follows the truncated Pareto distribution (40). The slope of the power law, β, characterizes the velocity heterogeneity of the fractured medium. As β decreases, the velocity heterogeneity increases. (b) Number n_c of correlation steps given by (35) as a function of parameter a for $N = 100$ velocity classes. By changing the value of the diagonal, a, we can systematically vary the strength of the velocity correlation from the uniform transition matrix that is equivalent to the uncorrelated velocity field to the identity matrix that represents a fully correlated velocity field.

$$\lambda = \frac{\ell}{r_c} \frac{1}{\ln\left(\frac{N-1}{Na-1}\right)} \overset{N\gg 1}{\approx} \frac{\ell}{r_c} \frac{1}{\ln\left(a^{-1}\right)}. \tag{39}$$

Thus, the correlation length λ is uniquely determined by the value of a.

For the steady state transition time distribution, $\psi(\eta)$, we use the truncated Pareto distribution,

$$\psi(\eta) = \frac{\beta \eta^{-1-\beta}}{\eta_\ell^{-\beta} - \eta_u^{-\beta}}, \eta_\ell < \eta \leq \eta_u. \tag{40}$$

We fix the mean of the transition time distribution to 1, which ensures that the mean arrival time in the correlated CTRW model (25c) is equal to the one in the homogeneous model (25b). Note that one could also choose to scale the peak arrival time with that of the homogeneous model, rather than fixing the mean arrival time. Furthermore, we enforce a given ratio of $r_\eta = \eta_u/\eta_\ell$ such that the power-law range covers the power-law regime observed in the breakthrough curves (see Figure 3). This determines η_ℓ as

$$\eta_\ell = \frac{1-\beta}{\beta} \frac{1 - r_\eta^{-\beta}}{r_\eta^{1-\beta} - 1}. \tag{41}$$

This bounds the value of η_ℓ between $\ln(r_\eta)/(r_\eta - 1)$, which is the limit of (41) for $\beta \to 0$, and $(r_\eta + 1)/(2r_\eta)$, which is the value of (41) for $\beta = 2$. For large contrasts $r_\eta \gg 1, \eta_\ell$ is approximately in $(\ln(r)/r, 1/2]$.

The transition time distribution (40) is illustrated in Figure 5. The slope β of the truncated Pareto distribution describes the heterogeneity of the velocity distribution. As β decreases, the transport becomes more anomalous because the probability of experiencing large transition times increases. Therefore, smaller β can be understood to represent higher flow heterogeneity, as is well known in the CTRW modeling framework [*Berkowitz et al.*, 2006].

In summary, the proposed transport model controls the velocity distribution and the velocity correlation with two independent parameters: the slope of the Pareto distribution, β, and the normalized correlation length λ.

4.3.2. Simulation of Convergent Tracer Tests

For the simulation of the convergent scenario, all the particles are injected at the injection well at $r_0 = r_i$, with r_i the radial distance between injection and pumping well. As discussed earlier, during the field tracer experiments, we flush the volume inside the packer with tracer-free fluid in order to ensure a sharp injection. Therefore, we use delta injection for both convergent and push-pull simulations. If the injection duration were not short enough to be approximated as a delta function, the simulation could be easily adapted by continuously releasing particles during the injection time. The convergent BTCs are obtained by recording the particle travel times at the well radius r_w of the pumping well at a radial distance of $r_c = r_i - r_w$. The detailed procedure is:

© 2014. American Geophysical Union. All Rights Reserved.

1. Assign the desired values to k_v, α, β, λ, and ℓ.

2. Simulate the sequence of particle positions and times according to (25a) and (25c).

3. Sample particle arrival times at r_w and obtain the BTC.

4.3.3. Simulation of Push-Pull Tracer Tests

The implementation for the push-pull scenario is similar to the one for the convergent scenario. Here, particles are injected at $r_0 = r_w$, with r_w the radius of the injection well. Particles travel radially outwards until the push duration t_{push}. Then, the radial direction is reversed and particles travel back to the injection well until they reach the well radius r_w. The algorithmic steps are identical to those of the convergent test, except that step 2 is split into its "push" phase and the flow reversal "pull" phase.

5. Model Behavior and Field Application

In this section, we study the model behavior of the proposed correlated CTRW model (25) depending on the three parameters α (dispersivity), β (velocity distribution), and λ (velocity correlation). We then apply the model to the experimental data presented in section 2 to explore the predictive capabilities of the model through the simultaneous prediction of BTCs in both convergent and push-pull tracer tests.

5.1. Model Behavior

We first consider the dependence of the peak arrival time on dispersivity α, the velocity distribution as parameterized by β, and the velocity correlation as parameterized by λ. Notice that the mean arrival time is the same in all cases because the model implementation detailed in the previous section forces the mean arrival of the correlated CTRW model (25c) to be equal to the one for the homogeneous CTRW model (25b). The minimum arrival time is obtained in the perfectly correlated CTRW, i.e., $a = 1$ in (37), which gives $\lambda = \infty$, and it is approximately

$$t_{\min} \approx \eta_\ell \frac{r_c^2}{2k_v}, \tag{42}$$

which can be obtained directly from (25c) by setting $\eta_n \equiv \eta_\ell$, the minimum nondimensional transition time. For the perfectly correlated model, the minimum arrival time is at the same time the peak arrival. As λ decreases, the peak arrival time increases due to loss of flow coherence, as illustrated in Figure 6a.

The simple estimate (42) for the fully correlated case also indicates how the peak arrival depends on β. Recall that η_ℓ depends on β as given in (41): it increases with increasing β up to a maximum of 1/2 for $\beta = 2$. From this, we conclude that the peak arrival time increases with increasing β, as illustrated in Figure 6. This

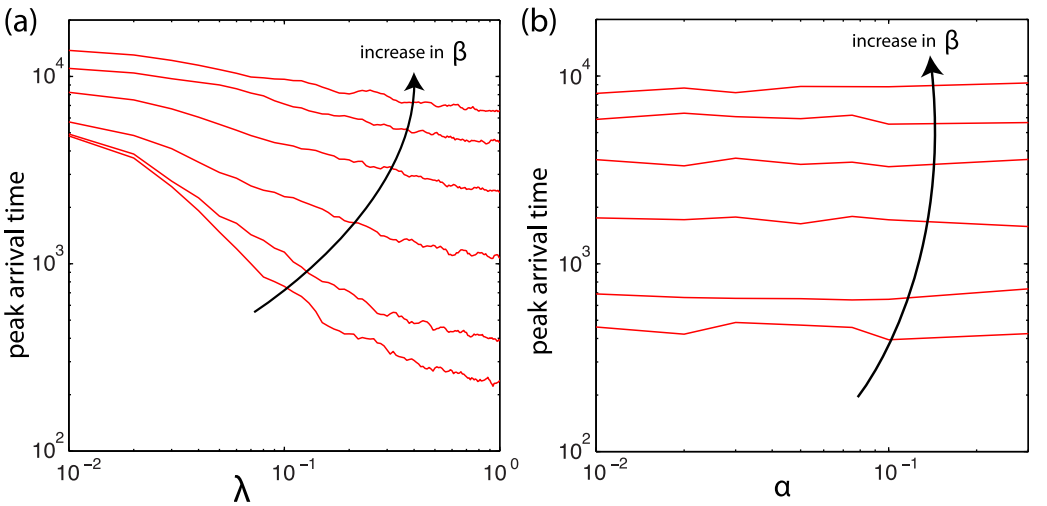


Figure 6. Sensitivity analysis for the peak arrival time on the three parameters of our CTRW model. (a) Change in peak arrival times for $\alpha = 0.3$ with varying λ. Different curves represent different degrees of velocity heterogeneity ($\beta = 0.5, 0.6, 0.8, 1, 1.2, 1.4$). (b) Change in peak arrival times for $\lambda = 0.2$ with varying α. Different curves represent different $\beta = 0.5, 0.6, 0.8, 1, 1.2, 1.4$.

© 2014. American Geophysical Union. All Rights Reserved.

may seem counterintuitive at first. Notice however, that we force the mean of $\psi(\eta)$ to be equal to 1 for a given range r_η. This means that as the probability of large transition times increases, η_ℓ must decrease as β becomes smaller.

Finally, the dispersivity α has essentially no impact on the peak arrival time, as illustrated in Figure 6b. This is intuitively clear when considering the mean arrival time (8) for the homogeneous model, which at the same time is the peak arrival time. It is completely independent of α, given that α only impacts the spreading about the mean arrival time.

In Figure 7, we plot tracer BTCs for a set of random walk particle tracking simulations for the convergent and push-pull scenarios for various combinations of α, β, and λ. Different features of the BTCs are sensitive to variation in α (dispersivity), β (velocity distribution), and λ (velocity correlation).

The dispersivity α mainly impacts the early time behavior of the convergent BTCs. As expected, a decrease in α leads to a slight decrease of the early arrivals due to the reduced particle dispersion (Figure 7a). Neither the late time tailing nor the peak position is affected by changes in α. For the push-pull scenario, a decrease in α decreases the relative dispersion of particle arrival times about the peak arrival times (Figure 7b). As for the push-pull test, the late-time scaling is not affected by the value of α.

For fixed λ, an increase in β leads to a decrease in BTC tailing in both the convergent and push-pull scenarios, as expected in the CTRW modeling framework [*Berkowitz et al*., 2006] (Figures 7c and 7d).

The correlation length λ impacts the early time BTC in the convergent scenario. We have already seen in Figure 6a that the peak arrival time increases with decreasing λ. Figure 7e shows that also the relative distance between the minimum arrival time and the peak arrival decreases with increasing λ. This behavior is caused by the fact that the particles sample a narrower window of the spectrum of transition times because of increased coherence. This leads to a decrease in the relative dispersion of early arrival times. For the push-pull scenario illustrated in Figure 7f, the impact of λ is more dramatic. The relative spread of arrival times about the peak arrival time decreases for increasing λ, which reflects the partial reversibility of the transport process in the presence of velocity correlation. In the limit of a perfectly correlated scenario for $\lambda=\infty$, i.e., $a = 1$ in (37), the BTC is identical to the one for a homogeneous medium, which is fully characterized by the dispersivity α (Figure 7f).

It is important to emphasize the difference between varying dispersivity α and correlation length λ. While increasing λ and decreasing α have qualitatively similar impacts on the relative early arrival times, their impacts on the BTC are very different. First, the peak arrival is essentially independent of dispersivity α, but depends strongly on correlation λ. Second, the limit $\lambda=\infty$ renders the BTC in the push-pull scenario identical to the one for a homogeneous medium because of full reversibility: no tailing is observed. For $\alpha = 0$, the strong BTC tailing in the push-pull scenario at long times remains unchanged.

5.2. Field Application

We now test whether our CTRW model with correlated velocities is able to capture the transport behavior observed in the field, as evidenced by the BTC in the tracer tests. In particular, we address the central question of whether tracer tests under different flow configurations (convergent and push-pull tests) can be explained with *the same* set of model parameters.

We perform a comprehensive comparison between the measured BTCs and the simulated BTCs over the entire three-dimensional space of possible parameter values for dispersivity α, velocity disorder β, and velocity correlation λ. We compute the unweighted mean square error (MSE), combined for the convergent, and push-pull tests over the entire range of measured data for each test.

The MSE surfaces for each of the fracture planes (B1-2 and B1-4) are shown in Figure 8 over the β-λ space, for a value of α close to the optimum. These surfaces show the existence of a single minimum in the MSE surface, corresponding to the optimum choice of model parameters that best matches *both* the convergent test and the push-pull test. These values are: $\alpha=0.03$[m], $\beta=0.75$[-], and $\lambda=0.22$[-] for fracture B1-2, $\alpha=0.02$[m], $\beta=0.85$[-], and $\lambda=0.06$[-] for fracture B1-4.

A weighted MSE can also be applied to estimate the set of parameters [*Chakraborty et al*., 2009]. This method utilizes the fact that concentration variance is proportional to concentration for the particle-

© 2014. American Geophysical Union. All Rights Reserved.

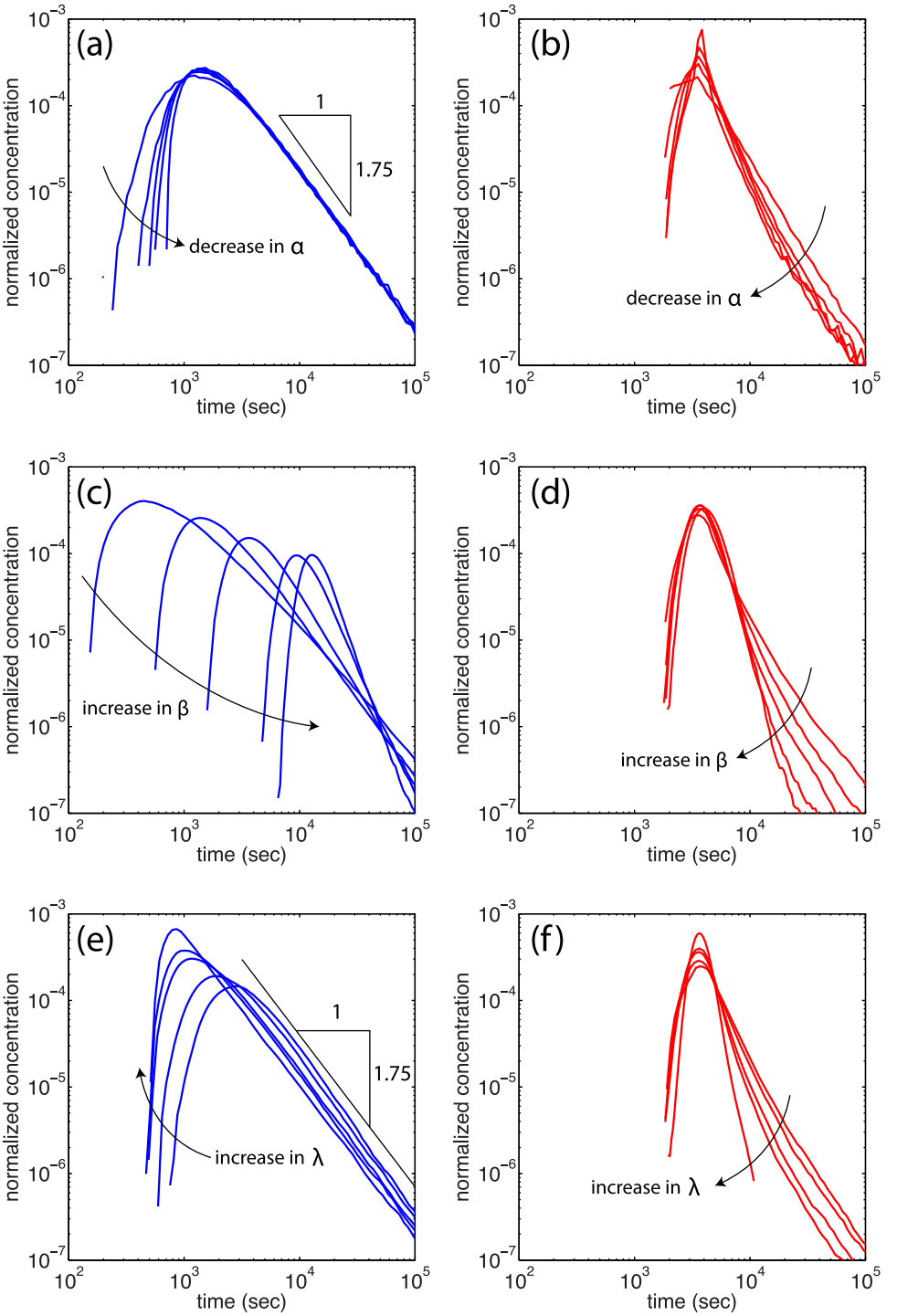


Figure 7. Impact of parameters α, β, and λ of our CTRW model on transport behavior. Left (a,c,e): convergent tests. Right (b,d,f): push-pull tests. Top (a,b): impact of dispersivity (α=0, 0.02, 0.05, 0.1, 0.3) for fixed β=0.75 and λ=0.2. Middle (c,d): impact of velocity distribution (β=0.5, 0.75, 1, 1.5, 2) for fixed value of α=0.03 and λ=0.2. Bottom (e,f): impact of velocity correlation (λ=0.05, 0.1, 0.3, 0.5, ∞) for fixed value of α=0.03 and β=0.75.

tracking model. The estimated parameters with the weighted MSE gave very similar set of parameters with unweighted MSE.

This suggests that B1-2 has similar dispersivity (α), slightly higher velocity disorder (smaller β), and significantly larger velocity correlation (larger λ) than B1-4. One way to qualitatively (but independently) confirm

© 2014. American Geophysical Union. All Rights Reserved.

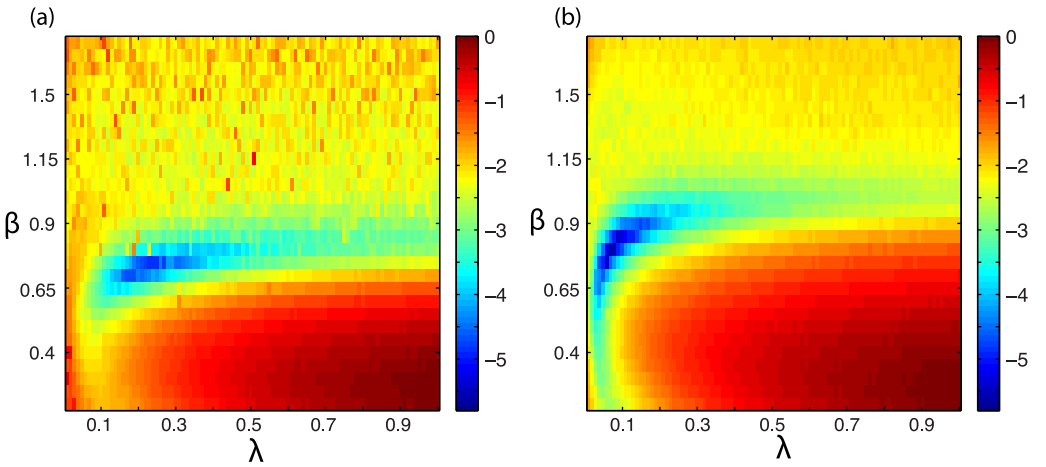


Figure 8. Plot of the mean square error (MSE) between modeled and measured BTCs for different model parameters. The error is for the combined differences of the convergent and push-pull tests. (a) MSE for the B1–2 fracture with a value α=0.03. The global minimum is for α=0.03, β=0.75 and λ=0.22. (b) MSE for the B1–4 fracture with a value α=0.02. The global minimum is for α=0.02, β=0.85 and λ=0.06.

this result is by comparing the characteristic fracture length in the field with the velocity correlation length inferred from our model. The estimated velocity correlation length from our model is ≈1.32 m for the B1-2 tracer test and ≈0.36 m for the B1-4 tracer test. Interestingly, this is of the same order of magnitude as the average distance between fracture connections measured independently by GPR imaging on the same site [*Dorn et al*., 2012]. This would suggest that fracture flow velocities are well correlated along connections with other fractures, and that they decorrelate mainly when changing fracture planes. However, this hypothesis cannot be confirmed from this data set alone.

The actual comparison between our model and the field data is shown in Figure 9. The proposed model accurately reproduces the BTCs of both push-pull and convergent tests (Figures 9a and 9b)—a quantitative agreement that is lost when neglecting velocity correlation (Figures 9c and 9d). Therefore, our one-dimensional CTRW with one-step correlation in velocity is a parsimonious, yet accurate, approximation for describing macroscopic transport in fractured media.

Although the model results explain the field experiment data from our campaign, the model has some limitations. In our modeling framework, we intrinsically assumed that the velocity distribution for the field of interest can be represented by a single probability distribution. However, if the study field is nonstationary, this assumption should be revisited. We also assumed that regional flow was negligible compared to the flow induced by pumping rates used in the field experiments. In our case, ambient flow rates were estimated from point dilution experiments and found to be two orders of magnitude smaller than injection and pumping rates. However, if ambient flow were large enough to affect the tracer experiment, this would influence the reversibility of the flow [*Lessoff and Konikow*, 1997; *Altman et al*., 2002]. If necessary, the modeling framework could be extended to incorporate nonstationarity and ambient flow.

6. Summary and Conclusions

In this study, we have proposed a unified framework to characterize transport in fractured media and account for both velocity distribution and velocity correlation. We first presented results from convergent and push-pull tracer tests in fractured-granite at the Ploemeur subsurface observatory (H+ network, France). The field data suggest that velocity distribution and velocity correlation are the key controlling transport properties. In particular, the BTCs recorded in the field demonstrate the more reversible character of tracer spreading for the push-pull test compared with the convergent test; an indication of the importance of velocity correlation.

Based on the field evidence, we have proposed a stochastic transport model that incorporates local dispersivity, Lagrangian velocity distribution, and Lagrangian velocity correlation as the three key transport processes, each characterized by a single parameter (α, β, and λ, respectively). We have shown analytically that our model embodies other existing models of transport as particular cases: it is equivalent to the MRMT

© 2014. American Geophysical Union. All Rights Reserved.

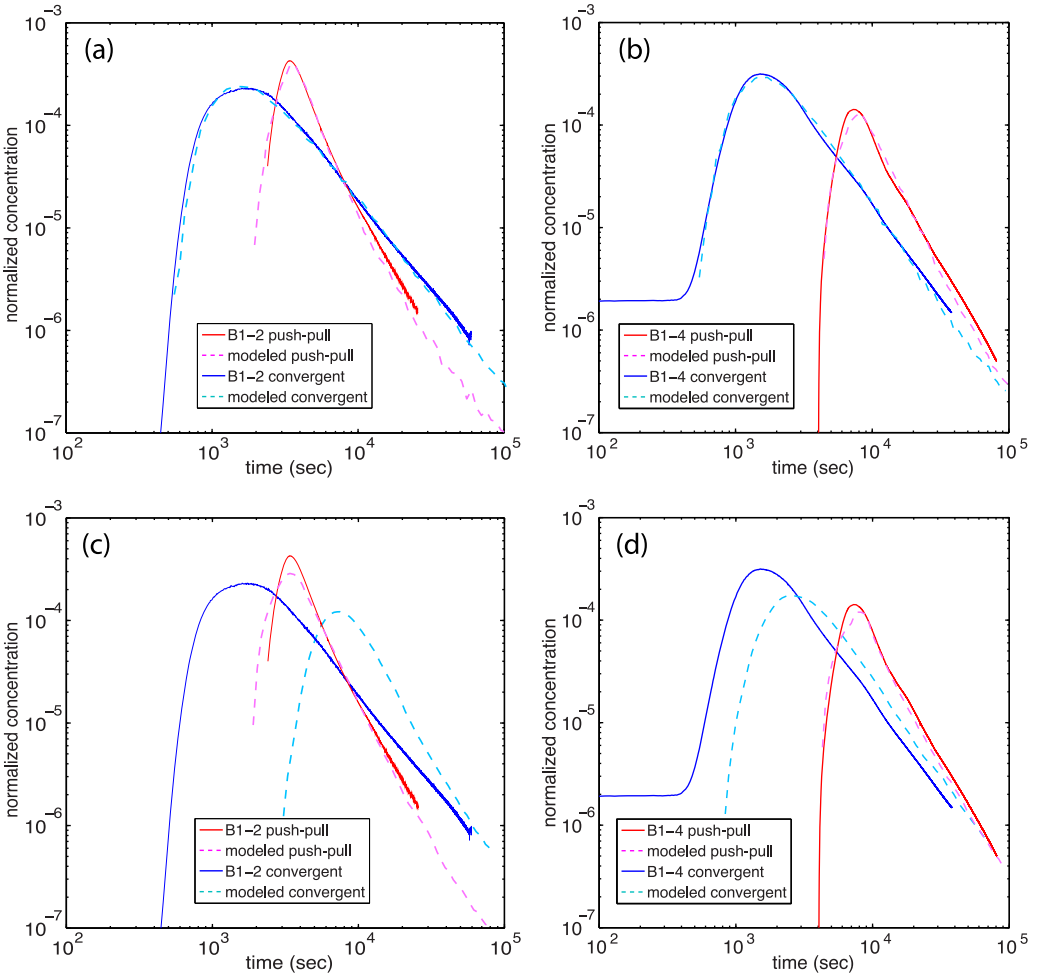


Figure 9. Comparison of measured and modeled BTCs for both convergent and push-pull tests, modeled with the same set of parameters. (a) B1–2 fracture; correlated CTRW model with parameters α=0.03, β=0.75, and λ=0.22. (b) B1–4 fracture; correlated CTRW model with parameters α=0.02, β=0.85, and λ=0.06. (c) B1–2 fracture; uncorrelated CTRW model with parameters α=0.03, β=0.95, and $\lambda = 0$. (d) B1–4 fracture; uncorrelated CTRW model with parameters α=0.02, β=0.65, and $\lambda = 0$.

model under the assumption of negligible velocity correlation, and to the SCST model under the assumption of infinite correlation.

In contrast, the correlated CTRW model proposed in this study is designed to capture the interplay between velocity distribution and velocity correlation, which we have illustrated with a sensitivity analysis of different metrics of the BTCs (early arrival time, peak arrival time, and late-time concentration decay) on the model parameters. The simplicity and versatility of our model has allowed us to perform a robust interpretation of the field tests, since the BTCs of both convergent and push-pull tests are retrieved accurately with the same set of parameters.

Our results raise important questions about modeling choices to simulate mixing and spreading in geologic media. For example, our model is designed to capture both push-pull and convergent BTCs with scale-independent local dispersivity, in contrast with the traditional Ansatz of a dispersivity that increases with the observational scale [*Gelhar et al.*, 1992]. Because our model accounts for macroscopic features with λ and β, it may permit removing the (spurious) scale dependence of local dispersivity α.

Finally, because the proposed model distinguishes between the spreading caused by advective processes (λ) and diffusive processes (α), we conjecture that it may provide an avenue to model not only tracer spreading but also fluid mixing [*Le Borgne et al.*, 2010, 2011; *Dentz et al.*, 2011b; *Jha et al.*, 2011; *de Dreuzy et al.*, 2012b; *Chiogna et al.*, 2012; *Jha et al.*, 2013]. The prediction of mixing and spreading rates in field-scale experiments remains, however, an exciting open question.

© 2014. American Geophysical Union. All Rights Reserved.

Acknowledgments
The authors thank Nicolas Lavenant and Rebecca Hochreutener for their help in setting up and running the field experiments. Our experimental data can be accessed at http://hplus.ore.fr/en. Funding for this work was provided by the INTERREG IV project CLIMAWAT, the national network of hydrogeological sites H+ (hplus.ore.fr). MD acknowledges the support of the European Research Council (ERC) through the project MHetScale (617511). R. J. acknowledges the support of the US Department of Energy (grant DE-SC0003907), and a MISTI Global Seed Funds award.

References

Altman, S. J., L. C. Meigs, T. L. Jones, and S. A. McKenna (2002), Controls of mass recovery rates in single-well injection-withdrawal tracer tests with a single-porosity, heterogeneous conceptualization, *Water Resour. Res.*, *38*(7), doi:10.1029/2000WR000182.

Becker, M. W., and A. M. Shapiro (2000), Tracer transport in fractured crystalline rock: Evidence of nondiffusive breakthrough tailing, *Water Resour. Res.*, *36*(7), 1677–1686.

Becker, M. W., and A. M. Shapiro (2003), Interpreting tracer breakthrough tailing from different forced-gradient tracer experiment configurations in fractured bedrock, *Water Resour. Res.*, *39*(1), 1024, doi:10.1029/2001WR001190.

Benke, R., and S. Painter (2003), Modeling conservative tracer transport in fracture networks with a hybrid approach based on the Boltzmann transport equation, *Water Resour. Res.*, *39*(11), 1324, doi:10.1029/2003WR001966.

Benson, D. A., and M. M. Meerschaert (2009), A simple and efficient random walk solution of multi-rate mobile/immobile mass transport equations, *Adv. Water Resour.*, *32*, 532–539.

Benson, D. A., S. W. Wheatcraft, and M. M. Meerschaert (2000), Application of a fractional advection-dispersion equation, *Water Resour. Res.*, *36*(6), 1403–1412.

Berkowitz, B., and H. Scher (1997), Anomalous transport in random fracture networks, *Phys. Rev. Lett.*, *79*(20), 4038–4041.

Berkowitz, B., A. Cortis, M. Dentz, and H. Scher (2006), Modeling non-Fickian transport in geological formations as a continuous time random walk, *Rev. Geophys.*, *44*, RG2003, doi:10.1029/2005RG000178.

Bibby, R. (1981), Mass transport of solutes in dual-porosity media, *Water Resour. Res.*, *17*(4), 1075–1081.

Bijeljic, B., and M. J. Blunt (2006), Pore-scale modeling and continuous time random walk analysis of dispersion in porous media, *Water Resour. Res.*, *42*, W01202, doi:10.1029/2005WR004578.

Bodvarsson, G. S., W. B., R. Patterson, and D. Williams (1999), Overview of scientific investigations at Yucca Mountain: The potential repository for high-level nuclear waste, *J. Contam. Hydrol.*, *38*, 3–24.

Brouyère, S., J. Batlle-Aguilar, P. Goderniaux, and A. Dassargues (2008), A new tracer technique for monitoring groundwater fluxes: The finite volume point dilution method, *J. Contam. Hydrol.*, *95*(3), 121–140.

Brown, S., A. Caprihan, and R. Hardy (1998), Experimental observation of fluid flow channels in a single fracture, *J. Geophys. Res.*, *103*(B3), 5125–5132.

Cacas, M. C., E. Ledoux, G. de Marsily, A. Barbreau, P. Calmels, B. Gaillard, and R. Margritta (1990), Modeling fracture flow with a stochastic discrete fracture network: Calibration and validation. 2. The transport model, *Water Resour. Res.*, *26*(3), 491–500.

Carrera, J., X. Sánchez-Vila, I. Benet, A. Medina, G. A. Galarza, and J. Guimerá (1998), On matrix diffusion: formulations, solution methods and qualitative effects, *Hydrogeol. J.*, *6*, 178–190.

Chakraborty, P., M. M. Meerschaert, and C. Y. Lim (2009), Parameter estimation for fractional transport: A particle-tracking approach, *Water Resour. Res.*, *45*, W10415, doi:10.1029/2008WR007577.

Chiogna, G., D. L. Hochstetler, A. Bellin, P. K. Kitanidis, and M. Rolle (2012), Mixing, entropy and reactive solute transport, *Geophys. Res. Lett.*, *39*, L20405, doi:10.1029/2012GL053295.

Cirpka, O. A., and P. K. Kitanidis (2000), An advective-dispersive streamtube approach for the transfer of conservative tracer data to reactive transport, *Water Resour. Res.*, *36*(5), 1209–1220.

Cueto-Felgueroso, L., and R. Juanes (2013), Forecasting long-term gas production from shale, *Proc. Natl. Acad. Sci. U. S. A.*, *110*(49), 19,660–19,661.

Curtis, J. B. (2002), Fractured shale-gas systems, *AAPG Bull.*, *86*, 1921–1938.

Dagan, G., and E. Bressler (1979), Solute dispersion in unsaturated soil at field scale, I, Theory, *Soil Sci. Soc. Am. J.*, *43*, 461–466.

de Anna, P., T. Le Borgne, M. Dentz, A. M. Tartakovsky, D. Bolster, and P. Davy (2013), Flow intermittency, dispersion, and correlated continuous time random walks in porous media, *Phys. Rev. Lett.*, *110*, 184502.

de Dreuzy, J. R., P. Davy, and O. Bour (2001), Hydraulic properties of two-dimensional random fracture networks following a power law length distribution: 1. Effective connectivity, *Water Resour. Res.*, *37*(8), 2065–2078.

de Dreuzy, J. R., J. Bodin, H. L. Grand, P. Davy, D. Boulanger, A. Battais, O. Bour, P. Gouze, and G. Porel (2006), General database for ground water site information, *Groundwater*, *44*(5), 743–748.

de Dreuzy, J. R., Y. Méheust, and G. Pichot (2012a), Influence of fracture scale heterogeneity on the flow properties of three-dimensional discrete fracture networks (DFN), *J. Geophys. Res.*, *117*, B11207, doi:10.1029/2012JB009461.

de Dreuzy, J. R., J. Carrera, M. Dentz, and T. Le Borgne (2012b), Time evolution of mixing in heterogeneous porous media, *Water Resour. Res.*, *48*, W06511, doi:10.1029/2011WR011360.

Dentz, M., and B. Berkowitz (2003), Transport behavior of a passive solute in continuous time random walks and multirate mass transfer, *Water Resour. Res.*, *39*(5), 1111, doi:10.1029/2001WR001163.

Dentz, M., and D. Bolster (2010), Distribution- versus correlation-induced anomalous transport in quenched random velocity fields, *Phys. Rev. Lett.*, *105*, 244301.

Dentz, M., D. Bolster, and T. Le Borgne (2009), Concentration statistics for transport in random media, *Phys. Rev. E*, *80*, 010101(R).

Dentz, M., P. Gouze, and J. Carrera (2011a), Effective non-local reaction kinetics for transport in physically and chemically heterogeneous media, *J. Contam. Hydrol.*, *120-121*, 222–236.

Dentz, M., T. Le Borgne, A. Englert, and B. Bijeljic (2011b), Mixing, spreading and reaction in heterogeneous media: A brief review, *J. Contam. Hydrol.*, *120-121*, 1–17.

Dorn, C., N. Linde, T. Le Borgne, O. Bour, and M. Klepikova (2012), Inferring transport characteristics in a fractured rock aquifer by combining single-hole ground-penetrating radar reflection monitoring and tracer test data, *Water Resour. Res.*, *48*, W11521, doi:10.1029/2011WR011739.

Dorn, C., N. Linde, T. Le Borgne, O. Bour, and J.-R. de Dreuzy (2013), Conditioning of stochastic 3-D fracture networks to hydrological and geophysical data, *Adv. Water Resour.*, *62*, 79–89.

Feenstra, S., J. A. Cherry, and E. A. Sudicky (1985), Matrix diffusion effects on contaminant migration from an injection well in fractured sandstone, *Ground Water*, *22*(3), 307–316.

Geiger, S., A. Cortis, and J. T. Birkholzer (2010), Upscaling solute transport in naturally fractured porous media with the continuous time random walk method, *Water Resour. Res.*, *46*, W12530, doi:10.1029/2010WR009133.

Gelhar, L. W., C. Welty, and K. R. Rehfeldt (1992), A critical review of data on field-scale dispersion in aquifers, *Water Resour. Res.*, *28*(7), 1955–1974.

Gerke, H. H., and M. T. van Genuchten (1993), A dual-porosity model for simulating the preferential flow of water and solutes in structured porous media, *Water Resour. Res.*, *29*(2), 305–319.

© 2014. American Geophysical Union. All Rights Reserved.

Ginn, T. R. (2001), Stochastic-convective transport with nonlinear reactions and mixing: finite streamtube ensemble formulation for multicomponent reaction systems with intra-streamtube dispersion, *J. Contam. Hydrol.*, *47*, 1–28.
Haggerty, R., and S. M. Gorelick (1995), Multiple-rate mass transfer for modeling diffusion and surface reactions in media with pore-scale heterogeneity, *Water Resour. Res.*, *31*(10), 2383–2400.
Haggerty, R., S. W. Fleming, L. C. Meigs, and S. A. McKenna (2001), Tracer tests in a fractured dolomite 2. Analysis of mass transfer in single-well injection-withdrawal tests, *Water Resour. Res.*, *37*(5), 1129–1142.
Harvey, C. F., and S. M. Gorelick (1995), Temporal moment-generating equations: Modeling transport and mass transfer in heterogeneous aquifers, *Water Resour. Res.*, *31*(8), 1895–1911.
Huyakorn, P. S., S. Panday, and Y. S. Wu (1994), A three-dimensional multiphase flow model for assessing NAPL contamination in porous and fractured media, 1. Formulation, *J. Contam. Hydrol.*, *16*, 109–130.
Jha, B., L. Cueto-Felgueroso, and R. Juanes (2011), Fluid mixing from viscous fingering, *Phys. Rev. Lett.*, *106*, 194502.
Jha, B., L. Cueto-Felgueroso, and R. Juanes (2013), Synergetic fluid mixing from viscous fingering and alternating injection, *Phys. Rev. Lett.*, *111*, 144501.
Juanes, R., J. Samper, and J. Molinero (2002), A general and efficient formulation of fractures and boundary conditions in the finite element method, *Int. J. Numer. Meth. Eng.*, *54*(12), 1751–1774.
Kang, P. K., M. Dentz, T. Le Borgne, and R. Juanes (2011a), Spatial Markov model of anomalous transport through random lattice networks, *Phys. Rev. Lett.*, *107*, 180602, doi:10.1103/PhysRevLett.107.180602.
Kang, P. K., M. Dentz, and R. Juanes (2011b), Predictability of anomalous transport on lattice networks with quenched disorder, *Phys. Rev. E*, *83*, 030101(R).
Kang, P. K., P. de Anna, J. P. Nunes, B. Bijeljic, M. J. Blunt, and R. Juanes (2014), Pore-scale intermittent velocity structure underpinning anomalous transport through 3D porous media, *Geophys. Res. Lett.*, *41*, 6184–6190, doi:10.1002/2014GL061,475.
Karimi-Fard, M., L. J. Durlofsky, and K. Aziz (2004), An efficient discrete fracture model applicable for general purpose reservoir simulators, *Soc. Pet. Eng. J.*, *9*(2), 227–236.
Kazemi, H., L. S. Merrill, K. L. Porterfield, and P. R. Zeman (1976), Numerical simulation of water-oil flow in naturally fractured reservoirs, *Soc. Pet. Eng. J.*, *16*(6), 317–326.
Kerner, B. S. (1998), Experimental features of self-organization in traffic flow, *Phys. Rev. Lett.*, *81*(17), 3797–3800.
Kiraly, L. (1979), Remarques sur la simulation des failles et du réseau karstique par éléments finis dans les modèles d'écoulement, *Bull. Cent. Hydrogéol.*, *3*, 155–167.
Le Borgne, T., and O. Bour, J.-R. De Dreuzy, P. Davy, F. Touchard , (2004), Equivalent mean flow models relevant for fractured aquifers: Insights from a pumping tests scaling interpretation, *Water Resour. Res.*, *40*, WO5112, doi:10.1029/2003WR002436.
Le Borgne, T., and P. Gouze (2008), Non-Fickian dispersion in porous media: 2. Model validation from measurements at different scales, *Water Resour. Res.*, *44*, W06427, doi:10.1029/2007WR006279.
Le Borgne, T., et al. (2007), Comparison of alternative methodologies for identifying and characterizing preferential flow paths in heterogeneous aquifers, *J. Hydrol.*, *345*, 134–148.
Le Borgne, T., M. Dentz, and J. Carrera (2008), Lagrangian statistical model for transport in highly heterogeneous velocity fields, *Phys. Rev. Lett.*, *101*, 090601.
Le Borgne, T., M. Dentz, D. Bolster, J. Carrera, J.-R. de Dreuzy, and P. Davy (2010), Non-Fickian mixing: Temporal evolution of the scalar dissipation rate in heterogeneous porous media, *Adv. Water Resour.*, *33*(12), 1468–1475.
Le Borgne, T., M. Dentz, P. Davy, D. Bolster, J. Carrera, J.-R. de Dreuzy, and O. Bour (2011), Persistence of incomplete mixing: A key to anomalous transport, *Phys. Rev. E*, *84*, 015301(R).
Lessoff, S. C., and L. F. Konikow (1997), Ambiguity in measuring matrix diffusion with single-well injection/recovery tracer tests, *Groundwater*, *35*(1), 166–176.
Maloszewski, P., and A. Zuber (1985), On the theory of tracer experiments in fissured rocks with a porous matrix, *J. Hydrol.*, *79*(3-4), 333–358.
Martinez-Landa, L., and J. Carrera (2005), An analysis of hydraulic conductivity scale effects in granite (Full-scale Engineered Barrier Experiment (FEBEX), Grimsel, Switzerland), *Water Resour. Res.*, *41*, W03006, doi:10.1029/2004WR003458.
Martinez-Landa, L., J. Carrera, M. Dentz, D. Fernandez-Garcia, A. Nardi, and M. W. Saaltink (2012), Mixing induced reactive transport in fractured crystalline rocks, *Appl. Geochem.*, *27*(2), 479–489.
McKenna, S. A., L. C. Meigs, and R. Haggerty (2001), Tracer tests in a fractured dolomite 3. Double-porosity, multiple-rate mass transfer processes in convergent flow tracer tests, *Water Resour. Res.*, *37*(5), 1143–1154.
Méheust, Y., and J. Schmittbuhl (2000), Flow enhancement of a rough fracture, *Geophys. Res. Lett.*, *27*(18), 2989–2992.
Moench, A. F. (1995), Convergent radial dispersion in a double-porosity aquifer with fracture skin: analytical solution and application to a field experiment in fractured chalk, *Water Resour. Res.*, *31*(8), 1823–1835.
Molinero, J., and J. Samper (2006), Large-scale modeling of reactive solute transport in fracture zones of granitic bedrocks, *J. Contam. Hydrol.*, *82*, 293–318.
Molinero, J., J. Samper, and R. Juanes (2002), Numerical modeling of the transient hydrogeological response produced by tunnel construction in fractured bedrocks, *Eng. Geol.*, *64*(4), 369–386.
Moreno, L., and I. Neretnieks (1993), Fluid flow and solute transport in a network of channels, *J. Contam. Hydrol.*, *14*, 163–194.
Neretnieks, I. (1983), A note on fracture flow dispersion mechanisms in the ground, *Water Resour. Res.*, *19*(2), 364–370.
Neuman, S. P., C. L. Winter, and C. M. Newman (1987), Stochastic theory of field-scale Fickian dispersion in anisotropic porous media, *Water Resour. Res.*, *23*(3), 453–466.
Nicolaides, C., L. Cueto-Felgueroso, M. C. Gonzalez, and R. Juanes (2012), A metric of influential spreading during contagion dynamics through the air transportation network, *PLoS One*, *7*(7), e40961.
Nordqvist, A. W., Y. W. Tsang, C. F. Tsang, B. Dverstorp, and J. Andersson (1992), A variable aperture fracture network model for flow and transport in fractured rocks, *Water Resour. Res.*, *28*(6), 1703–1713.
Pruess, K. (2006), Enhanced geothermal systems (EGS) using CO_2 as working fluid: Novel approach for generating renewable energy with simultaneous sequestration of carbon, *Geothermics*, *35*, 351–367.
Reimus, P. W., and T. J. Callahan (2007), Matrix diffusion rates in fractured volcanic rocks at the Nevada Test Site: Evidence for a dominant influence of effective fracture apertures, *Water Resour. Res.*, *43*, W07421, doi:10.1029/2006WR005746.
Rinaldo, A., et al. (2012), Reassessment of the 2010-2011 Haiti cholera outbreak and rainfall-driven multiseason projections, *Proc. Natl. Acad. Sci. U. S. A.*, *109*(17), 6602–6607.
Risken, H. (1989), *The Fokker-Planck Equation*, Springer, Berlin.

© 2014. American Geophysical Union. All Rights Reserved.

Ruelleu, S., F. Moreau, O. Bour, D. Gapais, and G. Martelet (2010), Impact of gently dipping discontinuities on basement aquifer recharge: An example from Ploemeur (Brittany, France), *J. Appl. Geophys.*, *70*(2), 161–168.

Schmid, K. S., S. Geiger, and K. S. Sorbie (2013), Higher order FE-FV method on unstructured grids for transport and two-phase flow with variable viscosity in heterogeneous porous media, *J. Comput. Phys.*, *241*, 416–444.

Schumer, R., D. A. Benson, M. M. Meerschaert, and B. Baeumer (2003), Fractal mobile/immobile solute transport, *Water Resour. Res.*, *39*(10), 1022, doi:10.1029/2003WR002141.

Smart, P. L., and I. M. S. Laidlaw (1977), An evaluation of some fluorescent dyes for water tracing, *Water Resour. Res.*, *13*(1), 15–33.

Szulczewski, M. L., C. W. MacMinn, H. J. Herzog, and R. Juanes (2012), Lifetime of carbon capture and storage as a climate-change mitigation technology, *Proc. Natl. Acad. Sci. U. S. A.*, *109*(14), 5185–5189.

Tsang, Y. W. (1992), Usage of "equivalent apertures" for rock fractures as derived from hydraulic and tracer tests, *Water Resour. Res.*, *28*(5), 1451–1455.

Tsang, Y. W. (1995), Study of alternative tracer tests in characterizing transport in fractured rocks, *Geophys. Res. Lett.*, *22*(11), 1421–1424.

Tsang, Y. W., C. F. Tsang, I. Neretnieks, and L. Moreno (1988), Flow and tracer transport in fractured media: A variable aperture channel model and its properties, *Water Resour. Res.*, *24*(12), 2049–2060.

Tsang, Y. W., C. F. Tsang, F. V. Hale, and B. Dverstorp (1996), Tracer transport in a stochastic continuum model of fractured media, *Water Resour. Res.*, *32*(10), 3077–3092.

Wilking, J. N., V. Zaburdaev, M. D. Volder, R. Losick, M. P. Brenner, and D. A. Weitz (2013), Liquid transport facilitated by channels in Bacillus subtilis biofilms, *Proc. Natl. Acad. Sci. U. S. A.*, *110*(3), 848–852.

© 2014. American Geophysical Union. All Rights Reserved.